Electronic Supplementary Material (ESI) for Catalysis Science & Technology.

Supporting information for Early-Stage Particle Fragmentation Behavior of Silica-Supported Metallocene Catalysts

Silvia Zanoni, Nikolaos Nikolopoulos, Alexandre Welle, Aurélien Vantomme and Bert M. Weckhuysen

1. Fragmentation modes for olefin polymerization catalysts

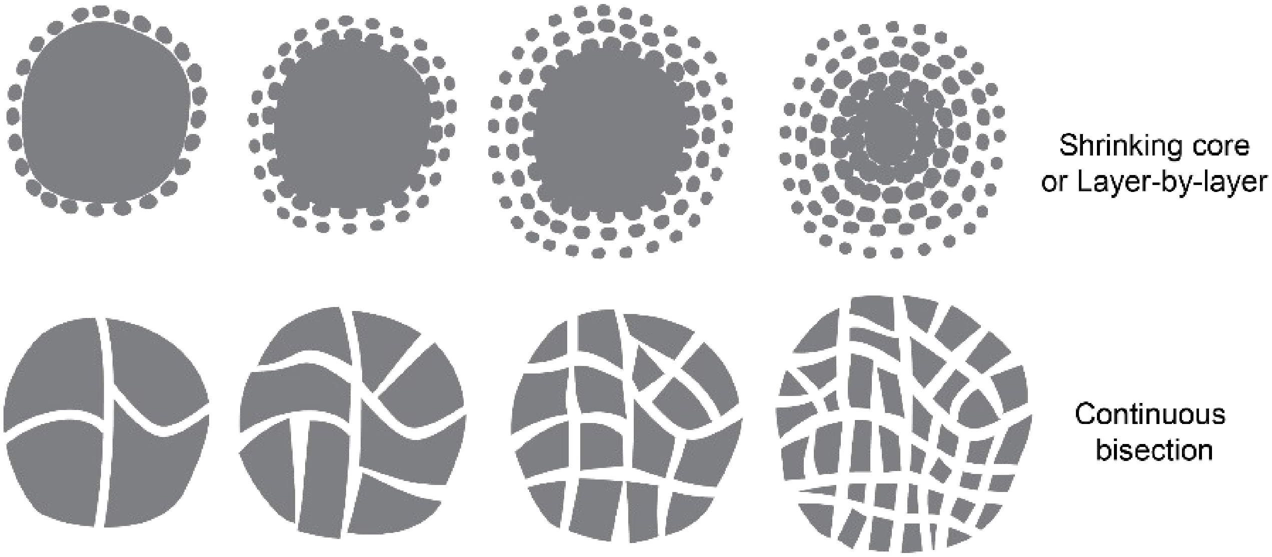

Figure S1: Schematic representation of the two fragmentation modes, shrinking core (or layer-by-layer) and continuous bisection.

2. Smallest fragment detectable size

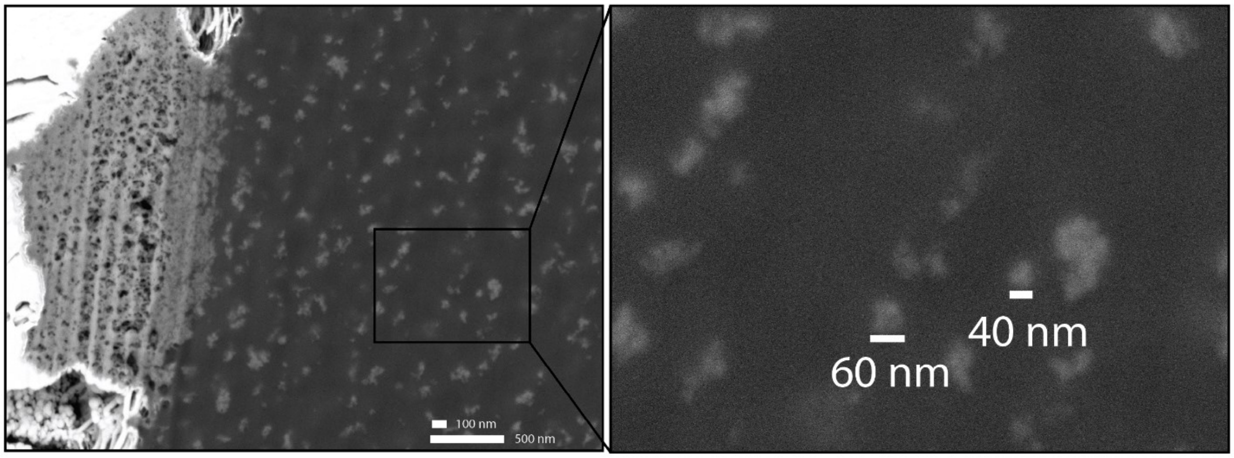

Figure S2: Cross-section of a polymerized metallocene-based catalyst particle with the deactivation of 1 um portion of the outer shell. Combining the Focused Ion Beam (FIB) precision milling and the high-resolution of the Scanning Electron Microscopy (SEM) allows for visualization of catalyst fragments as small as a few tens of nanometers embedded in the polymer phase.

3. Over-heating of sample in the gas phase

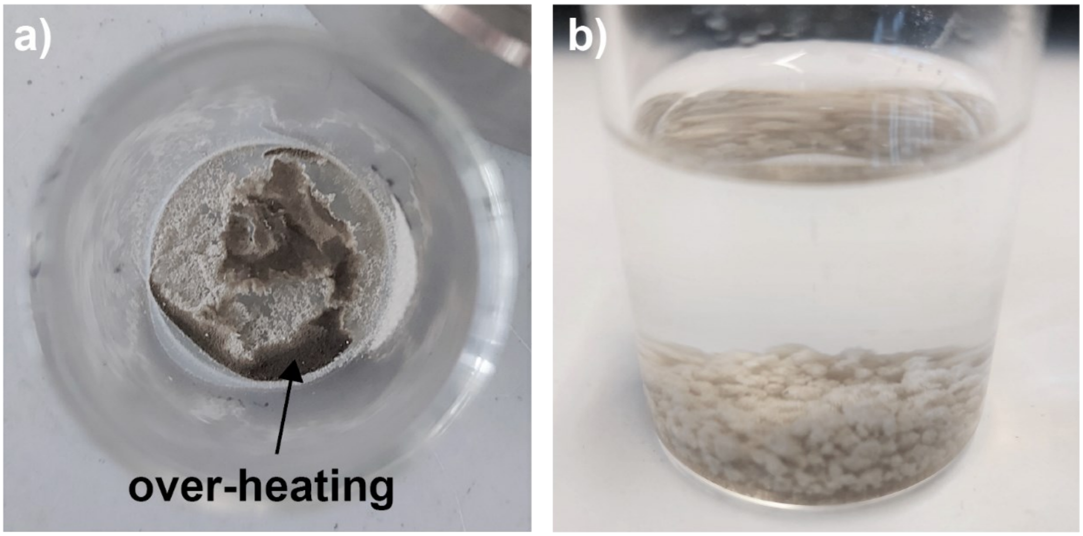

Figure S3: a) Catalyst particles polymerized in the gas-phase. The spots where multiple particles were overlapping experience severe over-heating. Hence care was taken to distribute the particles across the walls of the reactor quartz vial. b) catalyst particle polymerized in the slurry-phase where no over-heating is experienced thanks to the presence of a diluent.

4. Segmentation method

The segmentation of the 2D cross-section images was performed in Matlab with a K-means clustering, a method of signal processing that categorizes the pixels of the image into n clusters in which each pixel belongs to the cluster with the nearest mean (cluster centroid). More specifically, the pixels assignment to a cluster is based on obtaining the minimum possible sum of the squared distance between the data points and centroid. This also implies that less variation within the clusters leads to more similar data points within the same cluster; hence a higher contrast between polyethylene (PE) and catalyst material allows for better clustering.

In order to maximize the accuracy of image segmentation, only the top half of the catalyst particle was considered, as FIB-SEM creates a series of artifacts and material re-deposition on the lower portion of the FIB-milled section and pixels not belonging to the 2D cross-section plane were removed, i.e., background and pores. K-means clustering was then implemented with 4 was found to be the ideal number of centers.

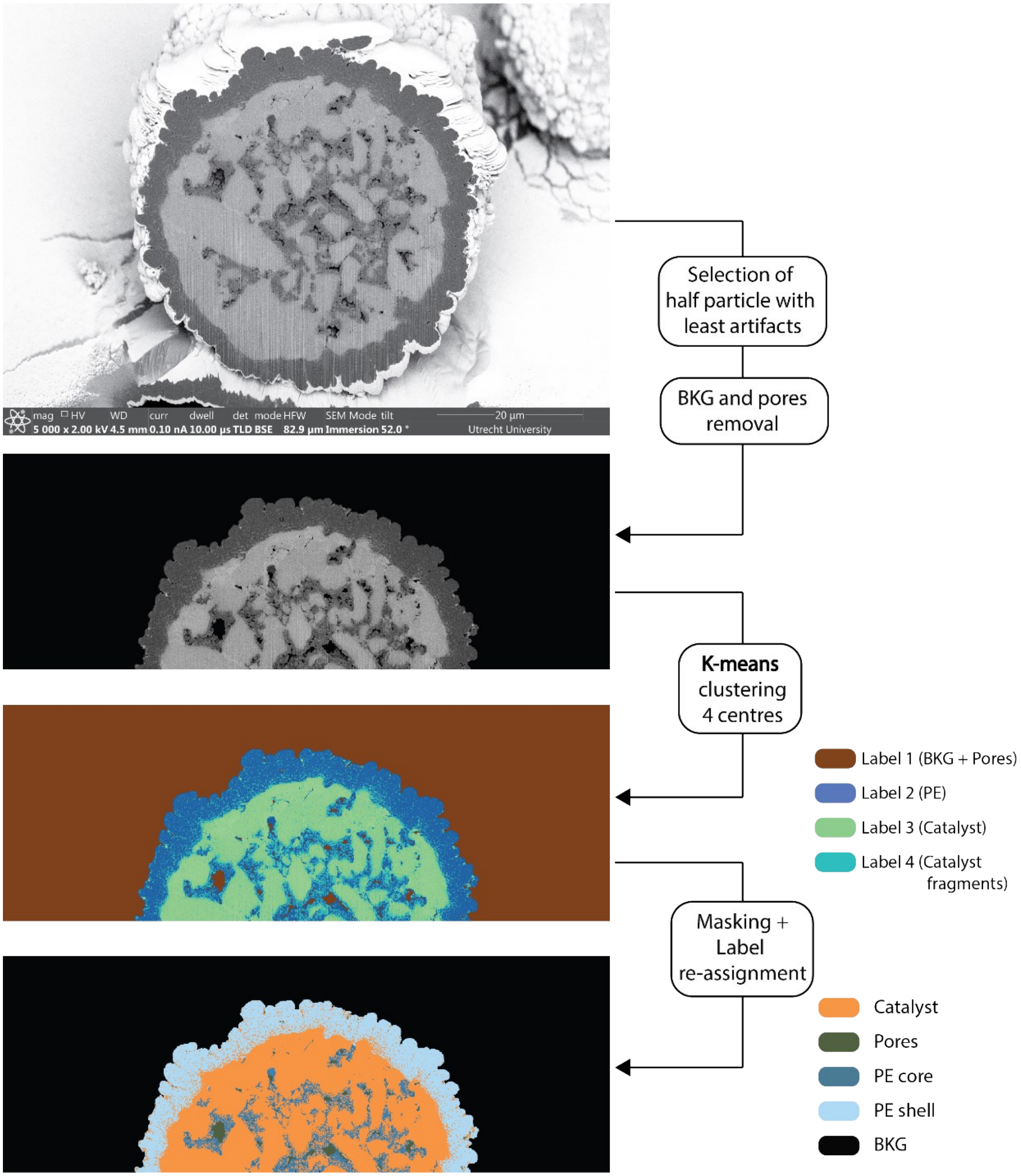

Figure S4: Image process analysis flow via the k-means clustering method.

5. K-meant method vs. manual thresholding

Image segmentation can also be performed by manual thresholding. Depending on the Scanning Electron Microscopy (SEM) collection settings of contrast and brightness, k-clustering might calculate centroids' positions in a non-reproducible way across the different samples. Therefore, manual thresholding was also applied and compared to the results from k-means clustering for all particles, and comparable results were obtained. Furthermore, manual thresholding has a margin of error related to the user's eye, so the delimiter point between two different phases can differ depending on the user's perception of the greyscale. The example below shows the comparison of the k-means method to two different manual thresholding. The difference in the % area of each component is minimal and does not affect the overall trends obtained for the entire series of samples analyzed. Thus, the two methods can be both effective in discerning catalyst and polymer in Focused Ion Beam (FIB)-SEM cross-sections.

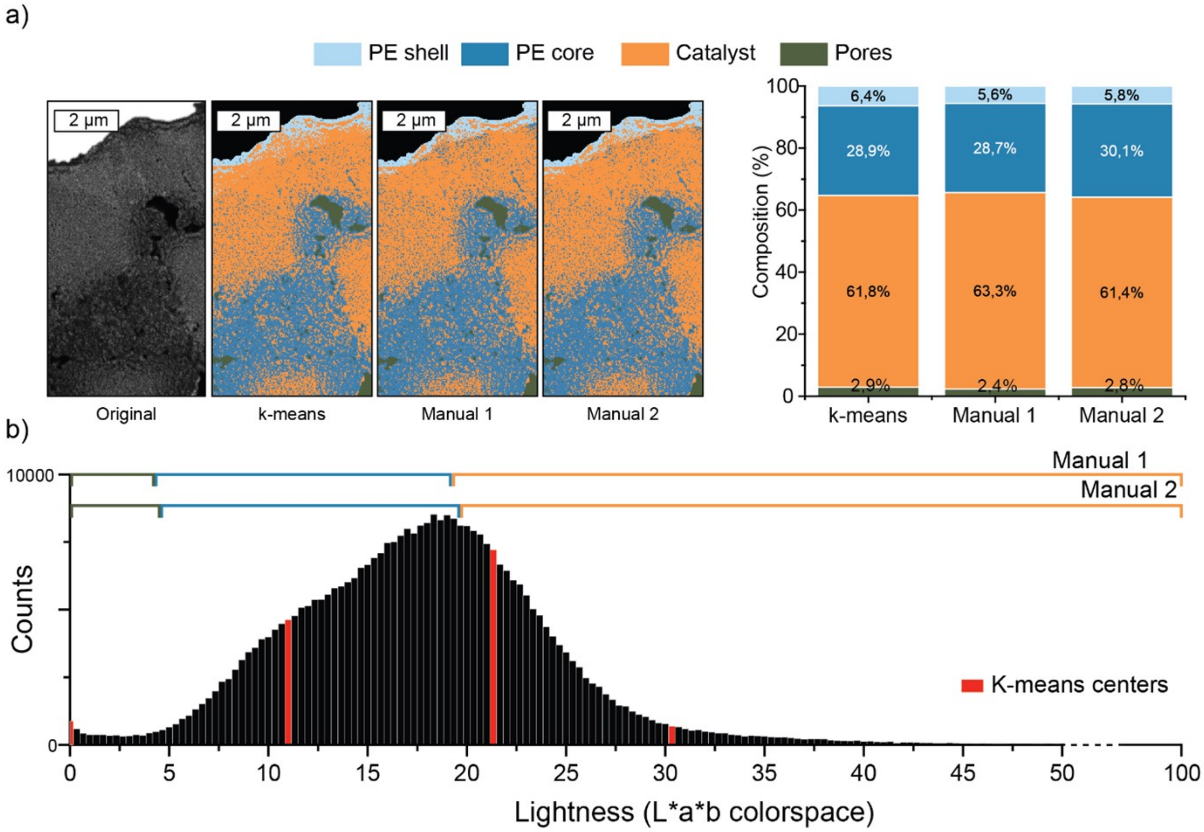

Figure S5: Image segmentation via the k-means clustering vs. the manual thresholding.

6. Pristine Catalyst morphology

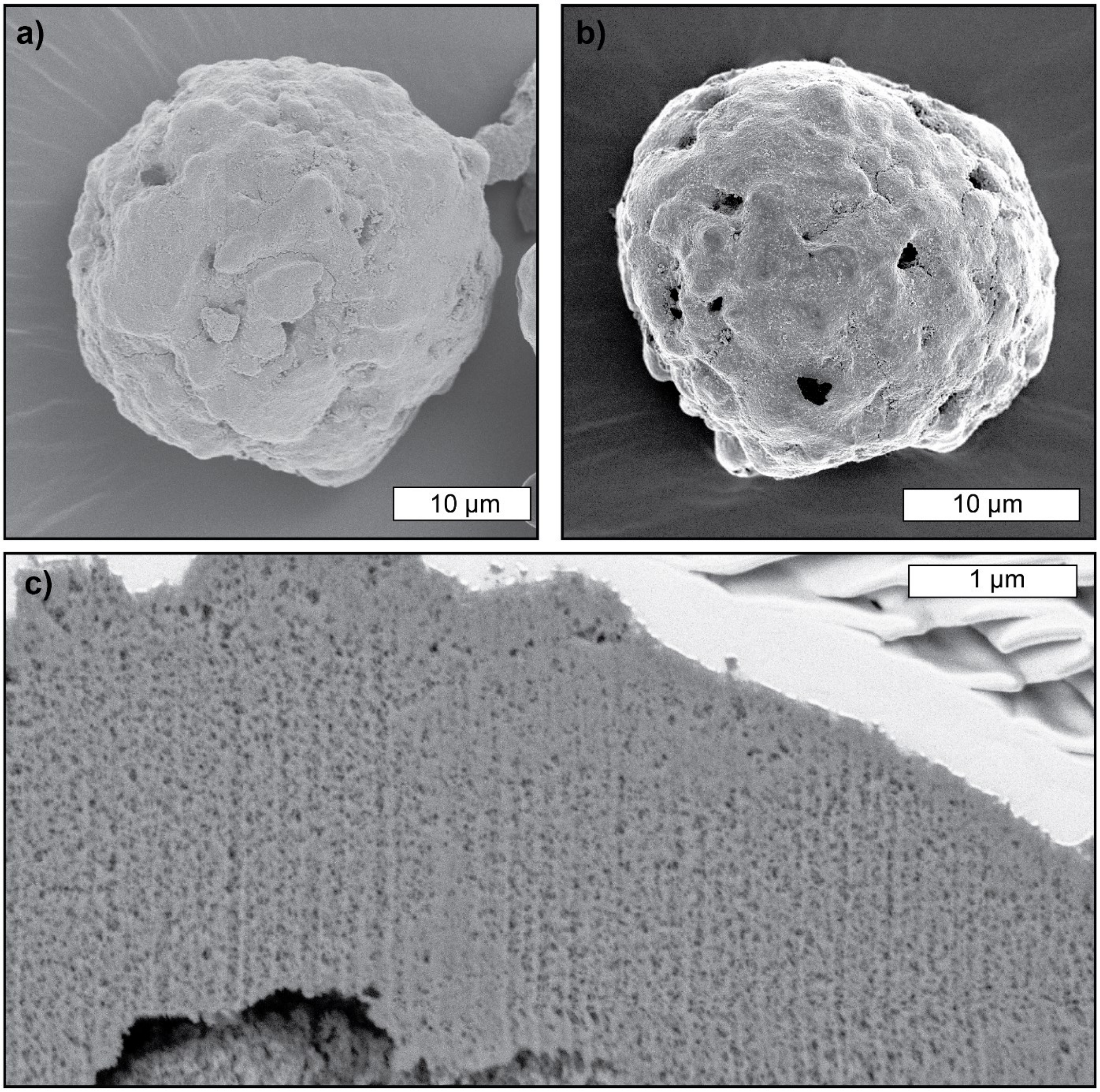

Figure S6: a,b) Scanning Electron Microgram of pristine catalyst particle outside morphology, where macropores are shown to be connected to the outer surface of the particles. c) Zoom-in of a pristine particle cross-section where the different densities of silica can be discerned.

The sample was first analyzed by N_2 physisorption at each stage of its synthesis, i.e. the bare SiO_2 support, after impregnation of the methylaluminoxane (MAO) co-catalyst and subsequent impregnation of the Zr metallocene catalyst. As reported in **Table S1** and **Figure S3**, the BET surface area is marginally increased with the addition of the co-catalyst, going from 219 m^2/g to 241 m^2/g, while the pore volume decreases by more than 50%. This is due to the grafting of MAO on the (internal and external) surface silanols of the SiO_2. The pore volume decreases as the SiO_2 pores are now filled with MAO, also shown by the pore size going from an average of 24 nm to 17 nm. On the other hand, the increase in surface area can be explained by the fact that the MAO layer is either *rougher* than pure silica or somewhat porous. The increase in surface area after MAO addition to the support has also been reported in the literature by Smit et al.[2] When the Zr catalyst is also added, the surface area marginally decreases, and the pore volume and size is slightly increased. This could be due to partial removal of MAO during the second impregnation procedure.

Table S1: BET surface area, total pore volume and average pore size of the analyzed samples by N_2 physisorption.

Sample	**BET[a] (m^2/g)**	**Pore volume[b] (cm^3/g)**	**Average pore size[c] (nm)**
SiO_2	219	1.44	24
SiO_2/MAO	241	0.65	17
SiO_2/MAO/Zr	220	0.66	17

[a]BET method, [b]single-point pore volume at p/p_o=0.95, [c]BJH desorption.

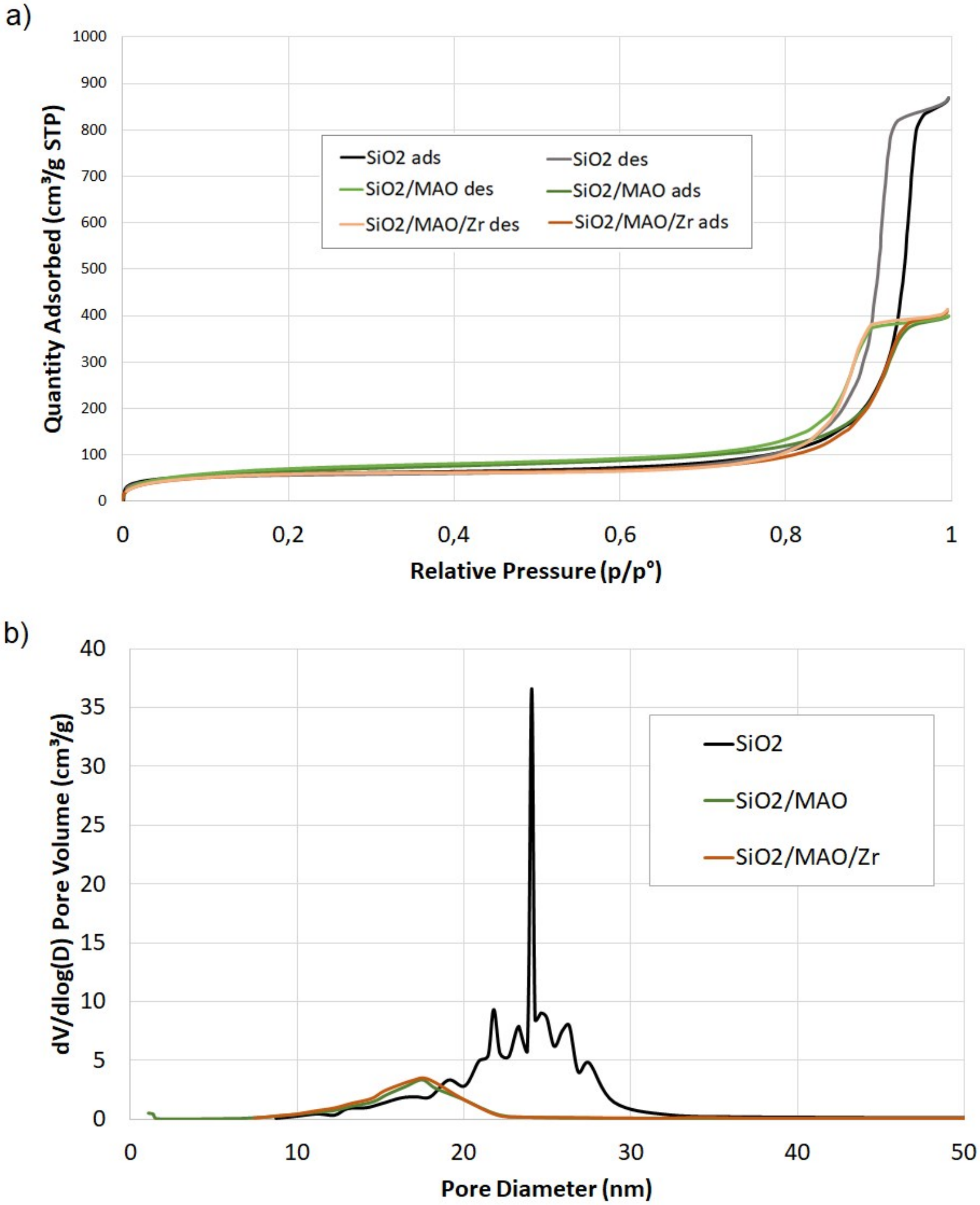

Figure S7: a) N_2 physisorption isotherms of the SiO_2, SiO_2/MAO, and SiO_2/MAO/Metallocene systems under study and b)corresponding BJH desorption pore size distribution.

7. Energy-dispersive X-ray elemental map of the pristine metallocene-based olefin polymerization catalyst

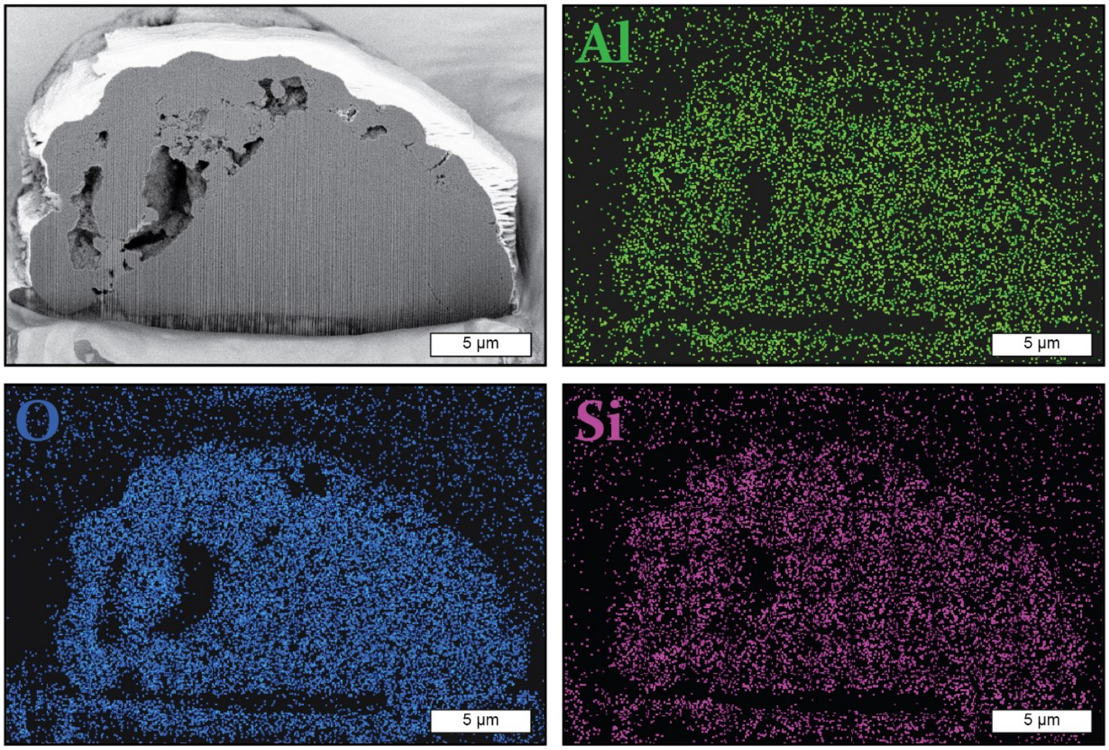

Figure S8: Scanning Electron Microscopy (SEM) of a pristine supported metallocene-based catalyst material and related Energy-Dispersive X-ray (EDX) elemental mapping through the particle cross-section. Al distribution confirms that the synthesis of the catalyst was successful in obtaining a homogeneous distribution of methylaluminoxane (MAO) co-catalyst throughout the catalyst particle.

8. Polymer yields for the metallocene-based catalyst under different reaction conditions

Table S2: Yield of polyethylene per gram of catalyst obtained at different reaction conditions.

Slurry/Gas	C_2H_4 pressure (bar)	Time (min)	Temp (°C)	Catalyst (mg)	Yield (g PE/g catalyst)
Gas	1	60	25	15.4	2.3
Gas	9	15	25	3.0	3.1
Gas	15	15	25	10.5	3.6
Slurry	15	5	25	10.0	9.4
				22.5	8.1
				11.2	6.3
Slurry	15	15	25	26.9	22.3
				22.7	22.4
Slurry	15	5	45	11.2	15.8
Slurry	15	5	60	10.2	23.3
Slurry (slow stirring)	15	15	25	23.1	2.2
Slurry (80 mg starting catalyst)	15	5	55 (average reached by exothermic reaction)	81.9	19.6
				80.8	19.0

9. Additional data on the supported metallocene-based ethylene polymerization catalyst

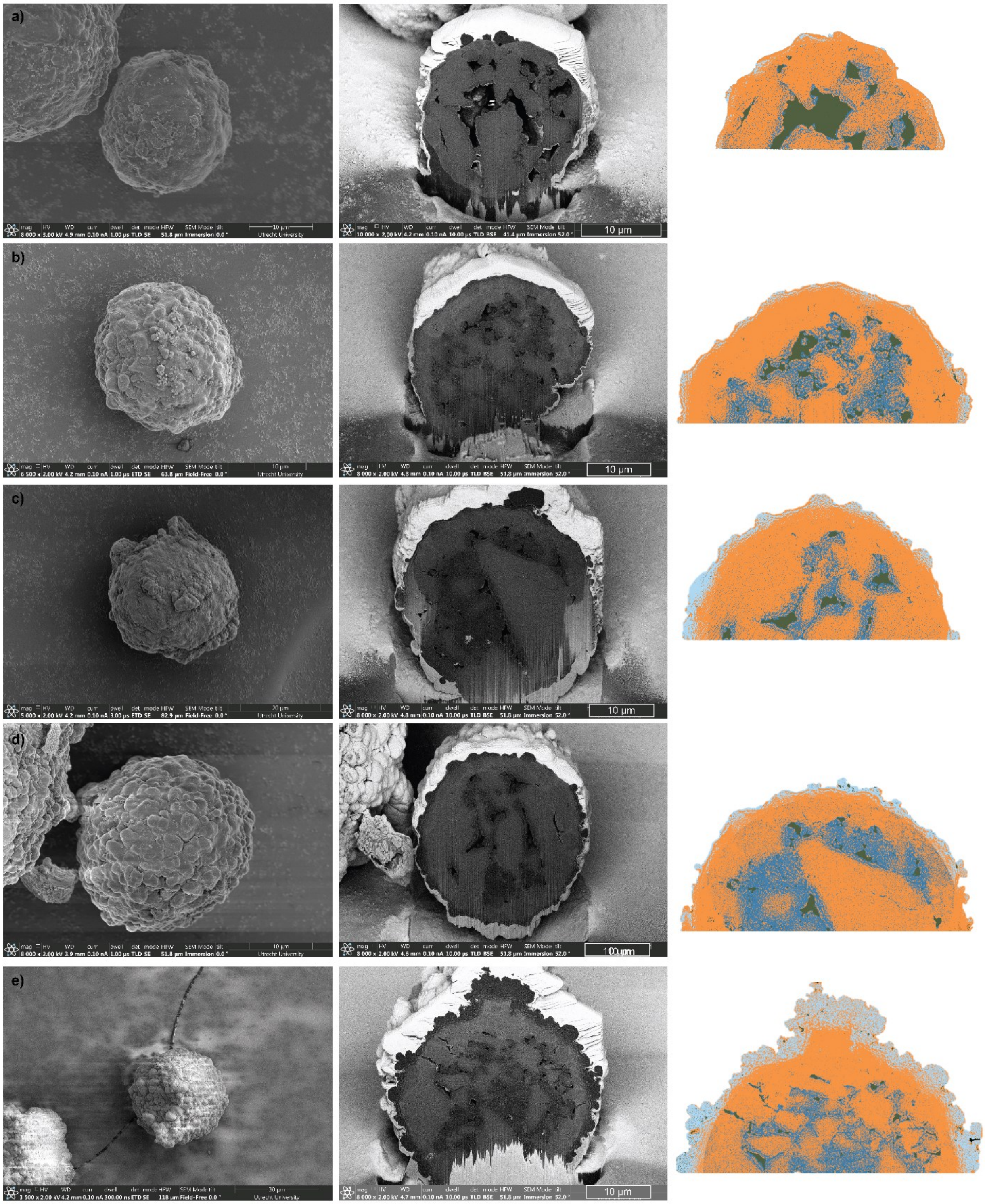

Figure S9: Scanning Electron Micrograms of external particle morphologies, Focused Ion Beam-SEM (FIB-SEM) cross-section images and corresponding segmentation of supported metallocene-based catalyst polymerized at 1 bar of ethylene pressure in the gas-phase for a) 5 min, b)15 min, c) 30 min, d) 45 min and e) 60 min.

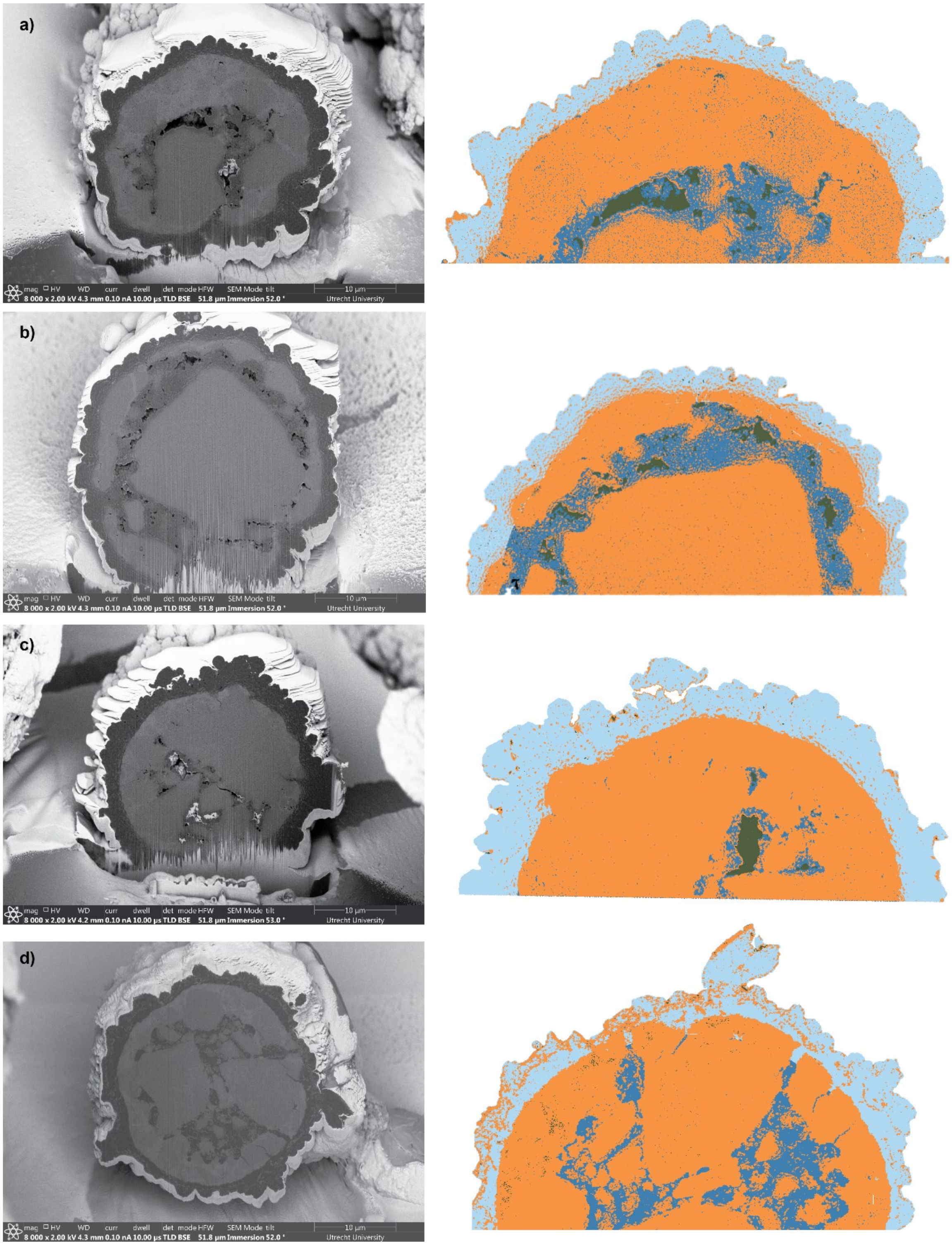

Figure S10: FIB-SEM cross-sections and corresponding segmentation of supported metallocene-based catalyst polymerized at a) 9 bar of ethylene pressure in the gas-phase for 15 min, b) at 15 bar of ethylene for 5 minutes, and c,d) for 15 minutes.

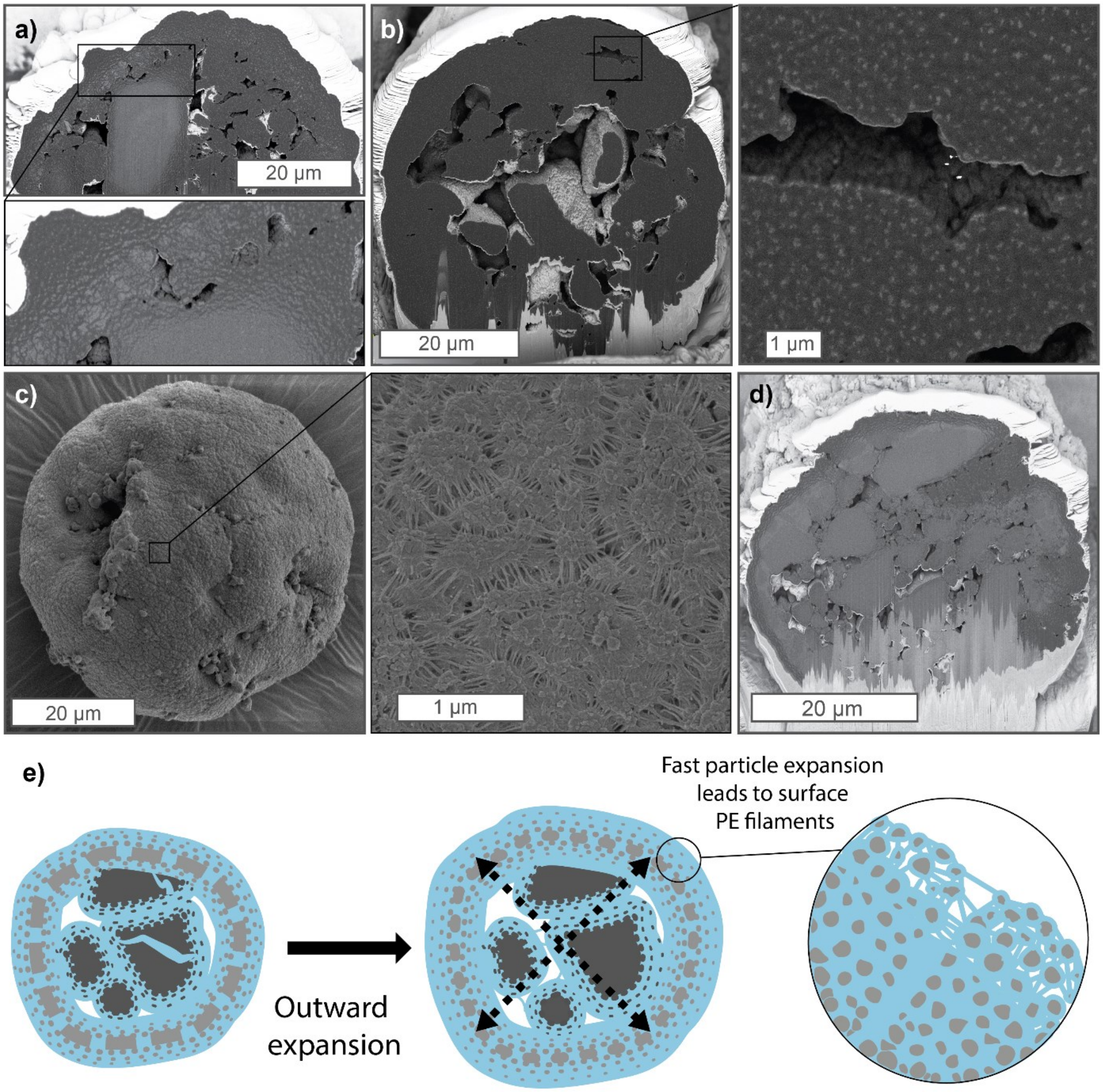

Figure S11: Focused-ion beam-scanning electron microscopy (FIB-SEM) cross-sections of supported metallocene-based catalyst polymerized in heptane at 15 bar of ethylene and room temperature (RT) with 400 rotations per minute (RPM) stirring performed a) for 5 min and b) 15 min and with the external morphology of the latter shown in c). d) Cross-section of a particle polymerized at 15 bar, RT for 15 min, with 60 RPM stirring speed. e) Schematic representation of catalyst particle fragmentation in slurry-phase at high pressures, where the catalyst is extensively and homogeneously fragmented; specifically, micrograins are drifting apart at the outer surface and from the mesoporous silica, with the dense silica shell first fragmenting in a sectioning mode. The particle expands, maintaining a level of macro- and mesoporosity that allows continuous access of the monomer to the active sites.

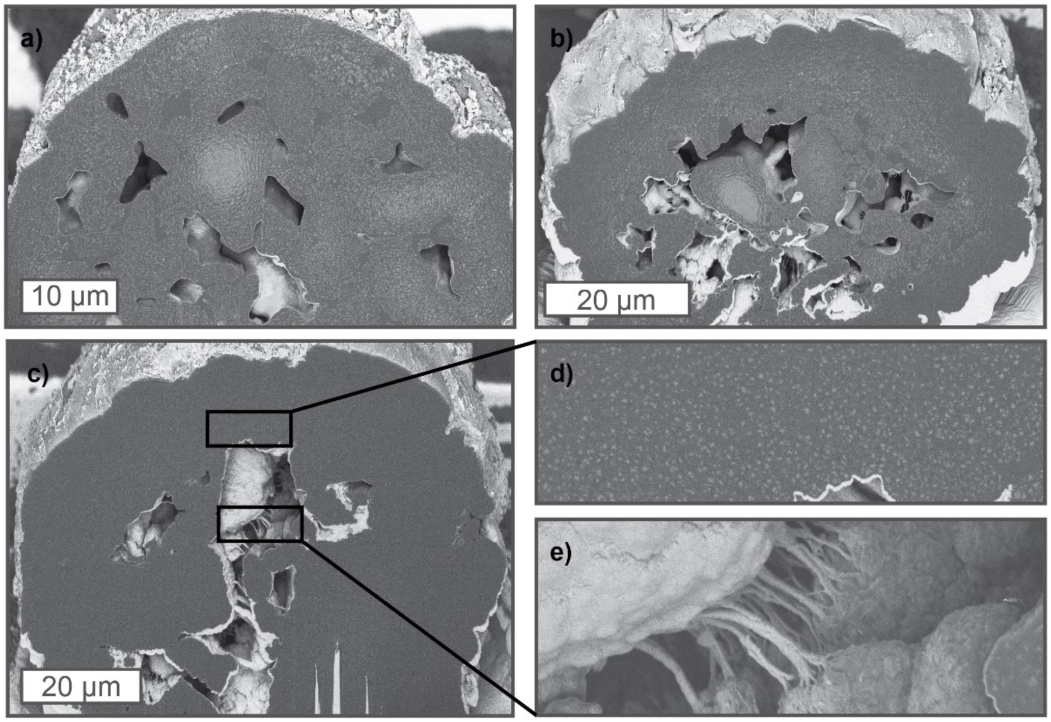

Figure S12: Focused Ion Beam-Scanning Electron Microscopy (FIB-SEM) cross-sections of supported metallocene-based catalyst polymerized in heptane at 15 bar of ethylene for 5 min at a) 25°C b) 45°C and c) 60°C, with zoom-ins of the latter shown in d-e.

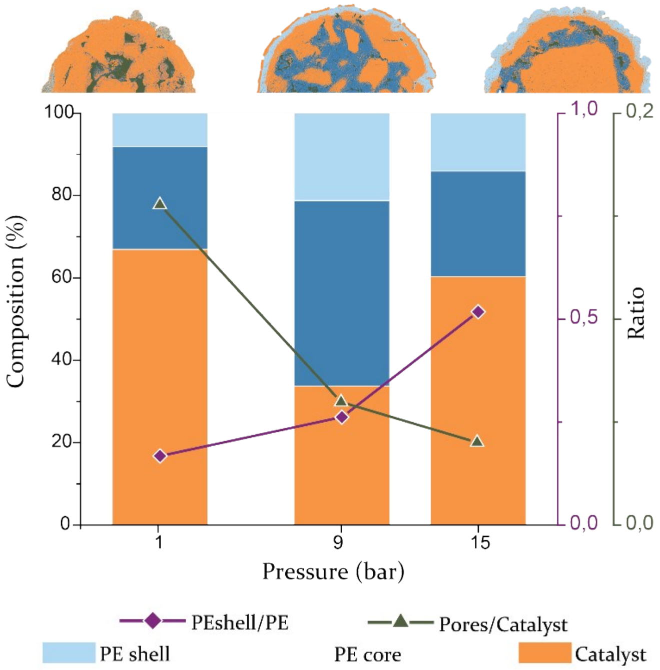

Figure S13: Segmentation of the cross-sections of the catalyst polymerized in the gas phase for 5 minutes as a function of ethylene pressure, with the correspondent areas % composition, PEshell/PE, and macropores/catalyst ratios. The sample polymerized at 9 bar exhibits partial deactivation of the shell, leading to the formation of external cracks and increased polymerization rates in the particle's core.

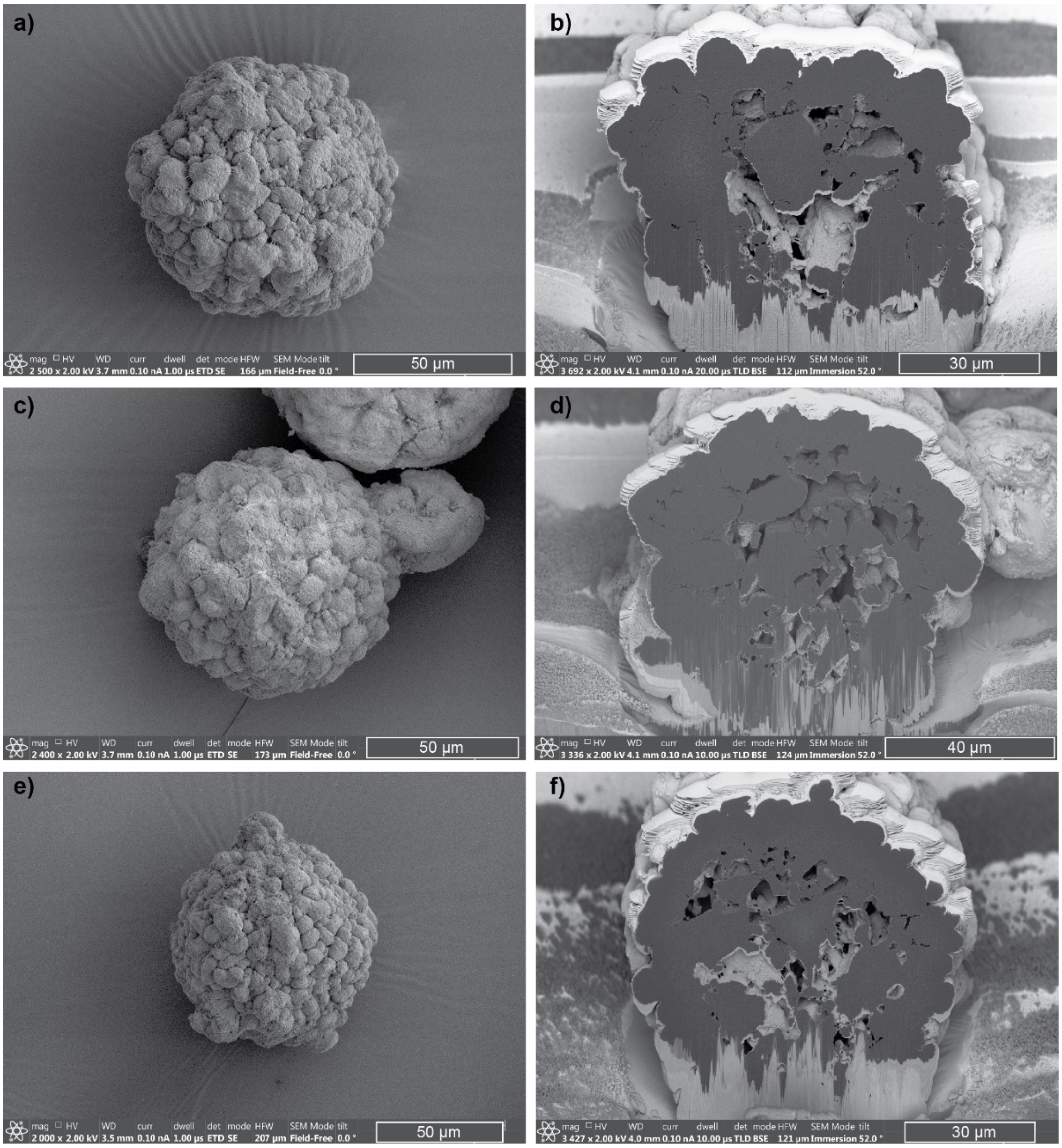

Figure S14: Scanning Electron microscopy (SEM) images of the outside morphology and Focused Ion Beam-SEM cross-sections of supported metallocene-based catalyst polymerized a,b) 15 bar of ethylene pressure in heptane for 5 min at 55°C, d,e,f) at 15 bar of ethylene pressure in heptane for 10 min at RT.